Solution Structure of a DNA Duplex Containing a *cis*-Diammineplatinum(II) 1,3-d(GTG) Intrastrand Cross-Link, a Major Adduct in Cells Treated with the Anticancer Drug Carboplatin†

Jan-Maarten Teuben,‡ Cornelia Bauer,§ Andrew H.-J. Wang,*,§ and Jan Reedijk*,‡

Leiden Institute of Chemistry, Gorlaeus Laboratories, Leiden University, P.O. Box 9502, 2300 RA Leiden, The Netherlands, and Department of Cell & Structural Biology and Department of Chemistry, University of Illinois at Urbana−Champaign, Urbana, Illinois 61801

Received March 1, 1999; Revised Manuscript Received May 26, 1999

ABSTRACT: The platinum 1,3-d(GXG) intrastrand cross-link is one of the adducts formed in the reaction of the antitumor drug cisplatin with DNA, and in fact the major adduct found in cells treated with the cisplatin analogue carboplatin. To determine the 3D structure of this adduct, the duplex d(CTCTG*TG*TCTC)·d(GAGACACAGAG)], where G*TG* denotes a platinum 1,3-intrastrand cross-link, was prepared and studied with high-resolution ^{1}H NMR. The solution structure was determined using the SPEDREF protocol, which includes an iterative NOE-restrained refinement procedure. Calculated and recorded NOE spectra were found to be in good agreement (NMR *R* factor 22%). The studied duplex is more distorted from B-DNA than previously determined structures of the 1,2-d(GG) intrastrand adducts. The base pairing is lost for the 5′G*-C and the central T-A base pair in the G*TG* lesion, and the central thymine is extruded from the minor groove. To accommodate this lesion, the minor groove is widened, and the 5′-guanine ribose adopts an N-type conformation. The helix is unwound locally and is significantly bent toward the major groove. Significant difference between the structural distortion of the 1,3-d(GTG) cross-link and other Pt−DNA cross-links sheds new light on the observed differences in protein recognition of these lesions, and thus on the possible differences in mechanisms of action of the various Pt−DNA adducts formed in treatment with platinum anticancer complexes.

The widely used antitumor agent cisplatin, [*cis*-diamminedichloroplatinum(II)][1], exerts its activity through formation of several types of adducts with DNA (*1*). Platinum adducts are known to distort the DNA severely. These distortions are subsequently thought to be recognized by proteins that mediate the cytotoxic activity (*2*). The major adduct (65%) is clearly the intrastrand 1,2-d(GG) cross-link, with minor incidences of 1,2-d(AG), 1,3-d(GXG), and interstrand cross-links for cisplatin (*3*). However, the relative occurrences of these adducts have been reported to be drastically different (*4, 5*) for carboplatin, [*cis*-diammine-(1,1-cyclobutyldicarboxylato)platinum(II)]. This cisplatin analogue, which only differs in the nature of its leaving group−cyclobutyldicarboxylate instead of two chlorides−yields the same DNA adducts as cisplatin. Interestingly, the distribution of Pt−DNA adducts formed with carboplatin, as determined in cells treated with carboplatin, appears to be 30% 1,2-d(GG), 16% 1,2-d(AG), 36% 1,3-d(GXG), and only 3−4% interstrand cross-links. The d(GXG) adduct is therefore the most abundant cross-link in cells treated with carboplatin. To this date, it remains unclear which of the Pt−DNA adducts is actually responsible for the biological activity of cisplatin, and it can even be disputed whether this activity can actually be completely pinpointed to any one of these adducts (*5*).

Increasing interest in the structural distortions of the various Pt−DNA adducts, in order to improve our understanding of protein recognition, has recently resulted in publication of a number of high-resolution solution NMR and X-ray structures of DNA duplexes containing platinum lesions (*7*). These studies have concentrated mainly on the 1,2-d(GG) intrastrand adduct (*7*−*10)*. The main distortions induced by this cross-link are bending of the helix toward the major groove by 55−78°, unwinding of the helix, and opening of the minor groove. Two recent solution structures show the platinated 5′G has a N-type sugar conformation commonly observed for A-DNA (*7*, *8*). As yet, the only available crystal structure of a platinated duplex reports an A/B DNA hybrid for a cisplatin d(GG) adduct. [Note added in proof: Two papers on crystal structures of cisplatin-

† This work has been performed with financial aid of The Netherlands Organization for the Advancement of Research (CW−NWO) to J. R., and the American Cancer Society (RPG-94−014−05) grant to A. H.-J. W. Additional support by the European Union (ERBCHRX-CT920014), and Cost action D8/0009/97 to J. R., and a NATO collaborative research grant 950734 to J. R. and A. H.-J. W. are gratefully acknowledged.

* To whom correspondence should be addressed.

‡ Leiden University (LIC).

§ University of Illinois (UIUC).

[1] Abbreviations: cisplatin, *cis*-diamminedichloroplatinum(II); carboplatin, *cis*-diammine(1,1-cyclobutyldicarboxylato)platinum(II); HMG high-mobility group; NOESY, nuclear Overhauser effect spectroscopy; TOCSY, total correlated spectroscopy; HPLC, high-performance liquid chromatography; rmsd, root-mean-square deviation; SPEDREF, spectral driven refinement.

10.1021/bi9904757 CCC: $18.00
Published on Web 08/27/1999

modified after this paper was submitted: the crystal structure of interstrand cross-linked DNA (*38*), and the crystal structure of a complex of an HMG domain with the major cisplatin d(GG) intrastrand adduct (*39*).] The A-form/B-form junction is located to the 3′ side of the platinum adduct. This hybrid A/B DNA nature of the duplex may arise from stacking interactions in the crystal, and may therefore not be present in solution (*9, 10*). A solution structure where a d(GG) site was reacted with *cis*-{Pt(NH_3)(4-aminoTEMPO)}$^{4+}$ has recently been solved, elegantly employing both diamagnetic and (long-range) paramagnetic NMR restraints. This structure revealed a similar tertiary structure as the previously determined cisplatin 1,2-d(GG) adducts (*11*).

To investigate the difference in structural distortion, attention has recently also focused on the other adducts formed in cisplatin treatment as well as on adducts of different platinum complexes. Two solution structures of the interstrand d(G)-d(G) cross-link have so far been reported (*12, 13*). The platinum atom in this adduct is located in the minor groove. The cytosines complementary to the platinated guanines were found to be extrahelical, and the duplex was bent toward the minor groove by ~45°. An interesting feature of the interstrand structure is that the helix is locally reversed to a left-handed form, resulting in an unwinding of about 80°. For the 1,3-d(GXG) adduct, an early model was presented based on NMR measurements and molecular modeling. This study reports that the helix is bent by 20°, and that the central thymine in the lesion is positioned in the minor groove, while it retains its stacking with the 5′G*- (*14*). Some of us (C.B. and A.H.-J.W.) recently reported how monofunctional platinum ammine complexes destabilize DNA (*15*). Together with the unusual dumbbell structure induced by an anticancer bisplatinum compound (*16*), this study shows that different platinum complexes may indeed distort the DNA in different manners. This observation might in fact explain their different antitumor properties, especially against cisplatin-resistant cells, and therefore a study of several complexes is desirable.

The importance of the differences in structural distortions of these adducts is highlighted by the findings that interactions with proteins are essentially different for the interstrand adducts, for the 1,3-d(GXG) adduct, and for the 1,2-d(GG) and 1,2-d(AG) adducts. The HMG1 protein selectively recognizes 1,2-d(GG) and 1,2-d(AG) cross-links, but not the 1,3-d(GXG) cross-links (*17, 18*). By shielding these two major adducts from repair, HMG proteins are believed to form a important step in the mode of action of cisplatin (*19*). In an earlier study, Donahue et al. (*20*) reported d(GG) and d(AG) cross-link specific recognition by a mammalian DNA recognition protein. Visse et al. (*21*) showed that DNA repair of these lesions also differs. They reported that incision by the *E. coli* UvrABC endonuclease is 3.5 times more efficient for 1,2-d(GG) adducts than for 1,3-d(GXG) adducts.

In an effort to better understand these differences, we investigated the structural distortion of a 1,3-d(GTG) adduct. In the present paper, we report the refined solution structure of a *cis*-diammineplatinum(II) 1,3-d(GTG) intrastrand cross-link in the double-stranded undecamer d(CTCTG*TG*TCTC)• d(GAGACACAGAG) (G* denotes N7 platinated guanines). We have employed the SPEDREF procedure for the determination of the tertiary structure of this adduct (*22*). This refinement procedure includes an iterative relaxation matrix refinement which drives the simulated and collected spectra to convergence. The implications of the structural distortions are discussed with respect to previously determined NMR and X-ray structures of the various Pt−DNA cross-links.

MATERIALS AND METHODS

Platination Reaction and Sample Preparation. The 11-mer oligonucleotides with the sequence d($C_1T_2C_3T_4G_5T_6G_7$-$T_8C_9T_{10}C_{11}$) (ssI) and its complement d($G_{22}A_{21}G_{20}A_{19}C_{18}$-$A_{17}C_{16}A_{15}G_{14}A_{13}G_{12}$) (ssII) were synthesized by the phosphoramidite method. After purification by preparative anion-exchange HPLC (Pharmacia Q Sepharose column, with a linear 0−1.2 M NaCl gradient in 0.02 M NaOH, pH 12), the solution was desalted with a gel filtration column (Pharmacia, Sephadex G25, DNA grade). The purity of the oligonucleotides was assessed using analytical anion exchange HPLC (Pharmacia, Mono Q column); subsequently a Dowex column (Sigma) was used to exchange the counterion to sodium.

cis-$PtCl_2(NH_3)_2$ was prepared according to Dhara (*23*). The deuterated monoaqua species was prepared by reacting cisplatin with 0.9 equiv of $AgNO_3$ overnight in the dark at room temperature in D_2O. A solution in 1 mL of D_2O of the purine-rich strand ssI (6 mg) was reacted with the deuterated monoaqua species of cisplatin in a 1:1 ratio at pH 3.8. The reaction was carried out in an NMR tube and monitored with ^{1}H NMR and HPLC (Pharmacia, Mono Q column, 20 min 0−1.2 M NaCl gradient at pH 12). After 3 days at RT, the reaction was judged to be complete, and the reaction mixture was purified as described above. The desired fractions were collected, neutralized with acetic acid, and lyophilized, yielding 2 mg of the platinated d($C_1T_2C_3T_4G_5$*T_6G_7*T_8C_9-$T_{10}C_{11}$) (ssIII), with the 1,3-intrastrand Pt−DNA cross-link.

The nonplatinated duplex I was prepared for comparison by titrating ssII to a solution of ssI in D_2O. Duplex formation was carried out at 288 K, monitored with ^{1}H NMR, and confirmed with anion HLPC run at pH 7. The same procedure was repeated with ssII and ssIII to produce the platinated duplex II. Both duplexes were lyophilized and redissolved 3 times with 99.8% D_2O, and finally redissolved in 250 μL of 99.96% D_2O. The solutions were transferred to an NMR tube, dried in a stream of nitrogen, and redissolved in 550 μL of 99.96% D_2O. For H_2O samples, duplex II was dissolved in 550 μL of 90% H_2O/10% D_2O. Final concentrations were 1.0 mM for duplex I, 0.7 mM for duplex II in D_2O, and 1.1 mM for duplex II samples in H_2O/D_2O. All samples contained 50 mM phosphate buffer, pH 7.

Electrospray mass spectrometry was performed using a FISONS/VG Quatro mass spectrometer at UIUC to confirm the nature of the platinum−DNA adduct; 0.1 mg of ssIII (NH_4^+ form) was dissolved in 1 mL of H_2O/2-propanol/0.4%NH_4OH, and injected into the flow system (50/50 acetonitrile/water) via a Rheodyne 7125 valve employing an ABI Model 104B pump at a flow rate of 10 μL/min. Data were acquired in the negative mode employing the VG MassLynx data system.

NMR Spectroscopy. Duplex formation was monitored on a VARIAN VXR 500 MHz at UIUC. T_1 relaxation experiments were carried out using the standard 180°−τ−90° inversion recovery sequence at 500 MHz. TOCSY spectra

were also recorded at 500 MHz. The platination reaction was monitored on a Bruker DMX 600 MHz spectrometer at LIC. All 2D spectra of duplex I, as well as phase-sensitive NOESY spectra of duplex II in H_2O buffer, were also acquired at 600 MHz, using the Watergate gradient pulse for minimization of the water signal (*24*). Phase-sensitive NOESY spectra in D_2O of duplex II were acquired on a Varian INOVA 750 MHz machine at UIUC. All 2D spectra were collected at 277 K with a mixing time of 200 ms. A total of 512 increments in t_1 were collected, each with 2048 complex data points in t_2, and 64 scans at a sweep width of 5000, 6000, and 7500 Hz using the 500 MHz, 600 MHz, and 750 MHz spectrometers, respectively. Spectra in H_2O were collected with a sweep width of 12 000 Hz.

All spectra were processed with FELIX (version 97.0, MSI, San Diego, CA), except for the 1D spectra measured on the Bruker DMX 600 MHz. These were processed using xwinNMR software (Bruker). For 2D spectra, the t_1 dimension was zero-filled to 2048 points and a polynomial base line correction was applied in the t_2 domain of the NOESY spectra. Chemical shifts were referenced to the HDO peak calibrated to a DSS (2,2-dimethyl-2-silapentanesulfonate) standard. The assignment aiding program ANSIG (*25*) was employed to aid assignments and to view and compare collected and simulated spectra.

Structural Refinement. Starting models of the platinated duplex d(CTCTG*TG*TCTC)·d(GAGACACAGAG) were constructed by docking *cis*-Pt$(NH_3)_2$ onto the N7 positions of G_5 and G_7 in the major groove B-DNA and A-DNA using QUANTA (version 4.0, MSI, San Diego, CA). A total of four starting models were assessed. Two models were based on B-DNA, and two models on A-DNA. For each family, one model was refined as constructed, and the other model was initially relaxed in X-PLOR version 3.8 (*26*), using conjugate gradient minimization. This initial minimization served to obtain correct geometries, especially of the Pt atom, and to obtain correct Pt−N distances. The minimization was performed without NOE restraints, using only planar restraints between base pairs. X-PLOR's all-atom force field with explicit hydrogen bond potentials was used. The force field for cisplatin was adapted to the X-PLOR format from Herman et al. (*27*).

NOE restrained refinement was performed according to the SPEDREF procedure (*22*). In this procedure, peak shapes and chemical shift values are fitted into the program MYLOR; the integrals from each NOE peak are consequently extracted automatically by evaluation with these peak shapes in the *f1* and *f2* dimensions. In each cycle of the SPEDREF procedure, the full relaxation matrix is calculated by the program MORASS (*28*). From the NOE relaxation rates, the corresponding NOE intensities are calculated using a mixing time (τ_m) of 200 ms. The isotropic correlation time (τ_c) was empirically determined to be 6 ns. Simulated spectra were subsequently calculated by the program CSL (in the SPEDREF package). NOE-restrained minimization cycles were run in XPLOR. Explicit base pair constraints were added for all base pairs, except for G_5*-C_{18} and T_6-A_{17}, since no base pairing for these pairs could be observed in the H_2O spectra. Repeating these cycles drives the simulated and experimental NOESY spectra to convergence. This convergence is represented by the NMR *R* factor which is defined as $\sum(N_o - N_c)/\sum N_o$, where N_o and N_c are the observed and calculated NOE intensities, respectively (*22*).

For each model, 40 cycles of the SPEDREF routine were applied to refine the structure. The molecule initially underwent 10 cycles of simulated annealing starting at 300 K. The temperature was lowered in 0.1 ps time steps to a temperature of 40 K. Each cycle was carried out for a total of 10 ps, after which the molecule was subjected to 80 steps of NOE restrained conjugate gradient minimization. During the last 30 cycles of the SPEDREF procedure, the molecule was refined with NOE restrained conjugate minimization only. Constant weighing of NOE restraints was applied throughout the whole procedure.

Both models for A-DNA as well as the initially nonrelaxed B-DNA yielded structures with grossly distorted geometries, with corresponding high chemical energy values and many NOE violations. *R* factors for each of these structures were ∼32%. The previously relaxed model based on B-DNA refined to an *R* factor of 22% and much lower chemical and NOE energies. For the final refinement, a family of 20 starting structures was created from this prerelaxed B-DNA model by simulated annealing for 1 ps at 300 K, followed by 1 ps in which the temperature was gradually lowered to 40 K. Each of these 20 starting structures was then submitted to the SPEDREF refinement procedure as described above.

RESULTS

Platination Experiments. The platination reaction of ssI with cisplatin was monitored with HPLC. The nonplatinated single strand (ssI), which is charged −10, eluted at 10.7 min. After addition of cisplatin, two additional peaks appeared at slower retention times, one corresponding to the monofunctional adduct (charge −9, at 10.2 min), and the other corresponding to the major product (ssIII, bearing a net charge of −8 at 9.2 min). After 3 days, the peak corresponding to the monofunctional adduct had almost completely disappeared, and the product was subsequently purified. The platination reaction was also monitored with NMR. A downfield shift of the H8 protons G_5 and G_7 indicated platination in 1D ^{1}H NMR spectra. These resonances shifted from 7.92 and 7.89 ppm to 8.33 and 8.31 ppm, respectively. These two new peaks can be assigned to the monoadducts. Within 20 h, the monoadduct had reacted to form the chelate, and two peaks at 8.32 and 8.19 ppm became dominant. These peaks could be assigned to ssIII, the 1,3-chelate (see Figure 1). After purification, the nature and purity of the ssIII were confirmed with electronspray mass spectrometry ($M = 3501$).

Duplex I and duplex II were prepared by titrating ssII to ssI and ssIII, respectively. Duplex formation was accompanied by the disappearance of resonances of the single strands (e.g., the methyl and the aromatic protons). Upon formation of duplex II, the resonances of the H8 protons of G_5* and G_7* shifted significantly: a large downfield shift to 8.85 ppm and an upfield shift to 7.86 ppm for the H8 protons of G_5* and G_7*, respectively, were observed. Both duplexes proved stable in solution for over 2 weeks at room temperature in the dark. Duplex stability was checked with 1D ^{1}H NMR. For duplex I, no significant broadening of the signals was observed until the duplex was heated to 333 K; similar broadening was observed for the platinated duplex II at 303 K already. This confirms that the 1,3-intrastrand

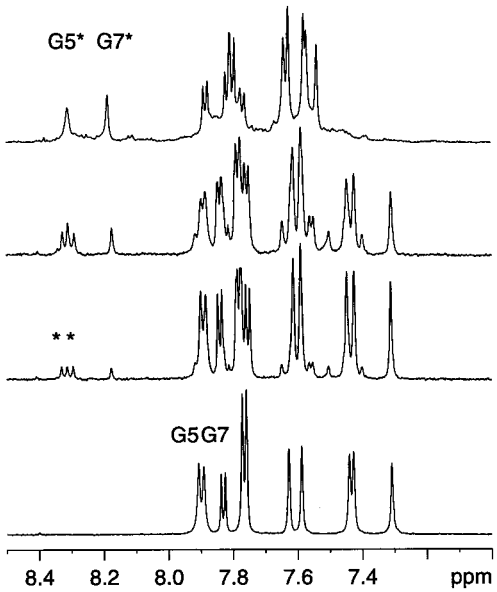

FIGURE 1: Aromatic region of ^{1}H NMR spectra of the platination reaction of ssI at $t = 0$ (bottom), after 1 h, 5 h, and 20 h (top). Peaks of the monofunctionally platinated guanines G_5* and G_7* are indicated with an asterisk; these have disappeared after 20 h, indicating the formation of the 1,3-chelate.

cross-link significantly reduces duplex stability (*14*, *33*). Imino protons and amino protons could be observed until 293 K, indicating that the oligonucleotide is still predominantly in duplex conformation.

NMR Analysis. Assignments of duplex I and duplex II were carried out according to the literature (*29*−*31*) and are listed in Table 1. The sequential assignment pattern is shown in Figure 2. The H2 protons could easily be identified from their long relaxation times in the T_1 relaxation experiment, and were assigned on basis of intraresidual H2 to H1′ cross-peaks and sequential *n* H2, (*n*+1) H1′ contacts. H2′ and H2″ sugar protons were assigned stereospecifically on the basis of the intensities of the H1′ to H2′/H2″ contacts (*32*). No stereospecific assignments were obtained for H5′ and H5″. For the unplatinated duplex I, the H2 and H5′ and H5″ protons were not assigned.

Assignment of the exchangeable protons of the platinated duplex II is based on connectivities to assigned nonexchangeable protons in the 200 ms NOESY in H_2O/D_2O. Only nine imino protons could be observed clearly. The imino resonances of G_5* and T_6 were initially not observed (see Figure 3). However, when the water signal was not suppressed, a weak peak for T_6 appeared at 11.68 ppm. The position of this peak is indicative of a T not involved in hydrogen bonding, in agreement with a similar ppm value observed for T_6 by van Garderen and van Houten (*14*), and an earlier NMR study by den Hartog et al. (*33*). The absence of cross-peaks for the imino protons of G_5* and T_6 in the 2D NOESY indicates that G_5* and T_6 are not involved in hydrogen bonding. All other imino protons exhibited cross-peaks in the 2D NOESY in H_2O/D_2O, although only one very weak contact to C_{11}NH1 was observed for G_{12}H1 (NH1 is assigned as the proton involved in hydrogen bonding). An unassigned cross-peak between two protons at 6.47 and 7.84 ppm is observed in the water spectrum. These protons exhibit no cross-peaks to other protons and can be tentatively assigned to amino protons of A_{17}.

Table 1: Chemical Shifts (ppm) of the Protons in Duplex I and Duplex II

	H8/ H6	H2/ H5/ Me	H1′	H2′	H2″	H3′	H4′	NH1/ NH2[b]	H1/ H3
				Duplex I					
C1	7.95	5.97	5.86	2.31	2.61	4.65	4.11		
T2	7.70	1.67	6.21	2.32	2.63	4.92	4.30		
C3	7.66	5.63	6.05	2.14	2.54	4.85	4.20		
T4	7.37	1.67	5.69	2.18	2.49	4.87	4.16		
G5	7.91		5.94	2.61	2.77	4.95	4.37		
T6	7.18	1.41	5.98	2.17	2.50	4.86	4.20		
G7	7.82		5.93	2.57	2.60	4.90	4.37		
T8	7.29	1.30	6.01	2.23	2.52	4.86	4.25		
C9	7.63	5.59	5.97	2.16	2.52	4.74	4.16		
T10	7.52	1.70	6.09	2.17	2.53	4.87	4.16		
C11	7.67	5.83	6.28	2.28	2.25	4.58	4.04		
G12	7.89		5.54	2.53	2.70	4.83	4.15		
A13	8.19	*a*	5.97	2.75	2.87	5.05	4.41		
G14	7.70	*a*	5.55	2.32	2.63	5.01	4.47		
A15	8.10	*a*	6.20	2.61	2.90	5.02	4.47		
C16	7.21	5.21	5.47	1.96	2.33	4.80	4.13		
A17	8.17	*a*	6.131	2.61	2.83	5.01	4.38		
C18	7.25	5.26	5.32	1.91	2.24	4.79	4.08		
A19	8.11	*a*	5.88	2.64	2.81	5.01	4.33		
G20	7.73		5.36	2.56	2.65	4.97	4.32		
A21	8.04	*a*	6.11	2.61	2.90	5.00	4.43		
G22	7.61		5.98	2.22	2.36	4.60	4.15		
				Duplex II					
C1	7.92	5.92	5.84	2.29	2.59	4.64	4.10	7.77/7.20	
T2	7.68	1.65	6.12	2.31	2.58	4.89	4.30		14.09
C3	7.66	5.61	6.02	2.17	2.57	4.81	4.17	8.53/7.25	
T4	7.48	1.71	6.08	2.15	2.53	4.88	4.15		14.16
G*5[d]	8.85		6.25	2.80	3.59	5.31	4.44		c
T6	7.90	2.00	6.30	2.56	2.67	5.11	4.39		11.68
G*7	7.86		5.78	2.55	2.62	4.79	4.10		12.91
T8	7.68	1.25	6.19	2.29	2.59	4.92	4.28		14.09
C9	7.61	5.63	6.02	2.06	2.41	4.81	4.15	8.46/7.24	
T10	7.40	1.64	5.95	1.95	1.80	4.72	4.15		13.99
C11	7.62	5.74	6.27	2.31	2.26	4.59	4.19	8.34/7.24	
G12	7.92		5.57	2.57	2.76	4.86	4.19		12.81
A13	8.22	7.75	5.99	2.78	2.90	5.08	4.43		
G14	7.77		5.60	2.65	2.75	5.04	4.43		12.67
A15	8.12	7.82	6.21	2.62	2.89	4.99	4.47		
C16	7.10	5.22	5.62	1.65	2.17	4.75	4.26	8.41/6.84	
A17	8.13	7.59	6.03	2.60	2.63	4.91	4.34		
C18	7.01	5.35	5.21	0.78	1.57	4.47	3.98	*c*	
A19	8.17	7.79	5.58	2.74	2.78	4.93	4.27		
G20	7.82		5.37	2.62	2.67	4.97	4.34		12.73
A21	8.13	6.14	6.19	2.66	2.95	5.05	4.14		
G22	7.66		6.13	2.17	2.49	4.64	4.28		13.40

[a] For the unplatinated duplex I H2, and exchangeable protons were not assigned. [b] NH1 is the proton involved in hydrogen bonding. [c] Not observed. [d] G* denotes platination of the guanine.

Qualitative Inspection of the NOE Data Already Revealed Information about the Tertiary Structure. The distortion at the G*TG* site in duplex II is immediately apparent from the absence of several sequential contacts normally observed for B DNA. In the 2D NOESY spectra of duplex I, all *n* H1′−(*n*+1)H8/H6 contacts could be identified except for the 3′-terminal T_{10}H1′−C_{11}H6 contact. Figure 2 shows the sequential assignment pathway for duplex II. These sequential contacts are missing between T_4-G_5* and T_6-G_7*, and it has a very small intensity for G_5*-T_6, implying that stacking interactions between G_5*, T_6, and G_7* are missing. In the complementary strand, the sequential connectivity pattern is disrupted between A_{17} and C_{18}, opposing the 5′ side of the Pt lesion. Another clear indication for distortion is the absence of the NOE contact between G_5*H6 and T_6CH_3 in

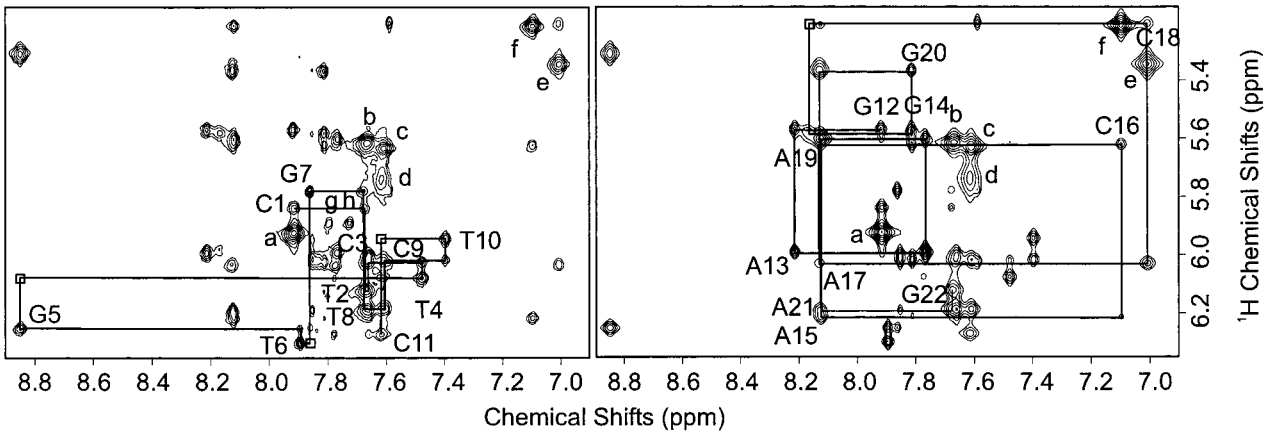

FIGURE 2: Comparison of contour plots of H6/H8 to H1′/H5 regions of experimental (left) and simulated (right) NOE spectra. The sequential assignment pathway for d($C_1T_2C_3T_4G_5$*T_6G_7*$T_8C_9T_{10}C_{11}$) is indicated in the experimental spectrum; the assignment pathway for the complementary strand d($G_{12}A_{13}G_{14}A_{15}C_{16}A_{17}C_{18}A_{19}G_{20}A_{21}G_{22}$) is indicated in the simulated spectrum. The missing connectivities are indicated with empty boxes. Cytidine H5/H6 cross-peaks are indicated: (a) C_1, (b) C_3, (c) C_9, (d) C_{11}, (e) C_{16}, (f) C_{18}. Cross-peaks labeled g and h arise from the presence of a slight excess of ssIII in the sample, and do not appear in the simulated spectrum.

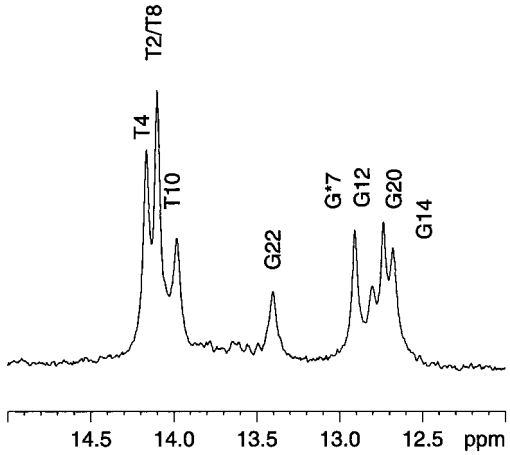

FIGURE 3: Imino region of a 1D exchangeable proton spectrum. Assignments of the nine observed imino protons are indicated.

duplex II. The ($n-1$)H8/H6−T_nCH$_3$ contacts are observed for all other thymines in duplex II and for all thymines in duplex I (Figure 4). These observations can be explained by our refined NMR model, where the T_6 is destacked and extruding from the helix. The observed cross-peak between G_5*H8 and G_7*H8 results from the close proximity of these protons due to platination at N7, as is confirmed by the weak NOE cross-peaks found between G_5*H1′/H2′ and G_7*H8 as well as G_5*H1′ and G_7*H1′. Other clear evidence for the local disruption of the helix is the absence of the cross-peaks to the imino protons of G_5*-T_6, as discussed above. A global indication of the localization of the structural distortions can be easily derived by comparing the chemical shifts of the platinated and unplatinated duplexes. These changes in chemical shift are summarized in Figure 5. Platination results in downfield shifts for certain protons, where others (mainly in the strand opposing the Pt adduct) exhibited upfield shifts. The H8 and H2″ of G_5* exhibit the largest downfield shift of 0.95 and 0.82 ppm, respectively. The H6 of T_6 shifts downfield by 0.71 ppm, whereas the H8 of the G_7* only shifts downfield by 0.04 ppm. These changes indicate that distortion from normal B DNA is most profound at the 5′ side of the Pt adduct, as also illustrated by the large upfield shifts of the C_{18} protons, the base opposing the 5′G_5* of the Pt adduct. The minor changes in the chemical shift values of the C_{20} protons (opposing the 3′G_7*) show that the distortion on the 3′ side of the lesion is less severe.

The conformations of the sugars could be deduced from the intensity of intraresidual H8/H6 to H3 cross-peaks, since the distance between these protons is 2.8−3.0 Å for an N-type conformation and 4.0−4.4 Å for the S-type conformation that is normally seen in B-DNA (*32*). This cross-peak has a medium to weak intensity for all residues, with the exceptions of G_5* and the 3′-terminal base C_{11}. This strong intensity for G_5*and C_{11} indicates that these bases have adopted an N-type conformation (Figure S1).

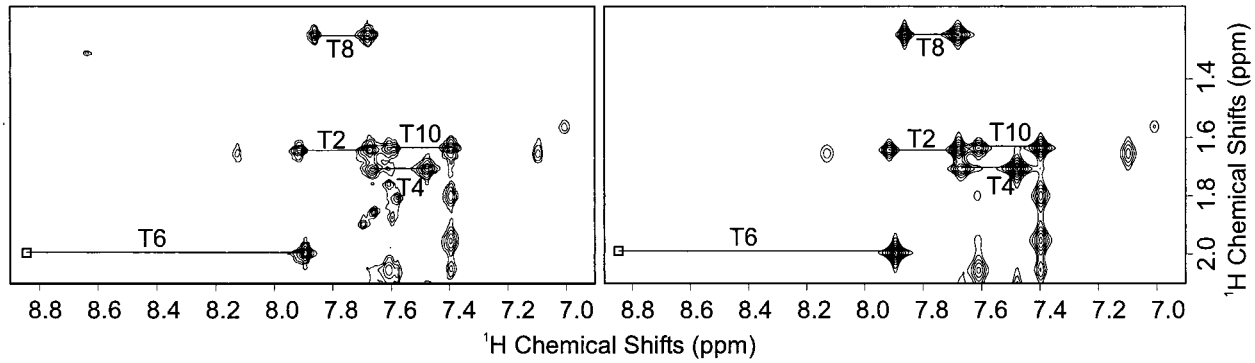

FIGURE 4: Contour plot showing the H6/H8 to methyl region of the experimental (left) and the simulated NOE spectra. Assignments of the methyl protons are indicated. Sequential NOEs are clear for all thymines, except for G_5* and T_6 (the missing cross-peak is illustrated with an empty box).

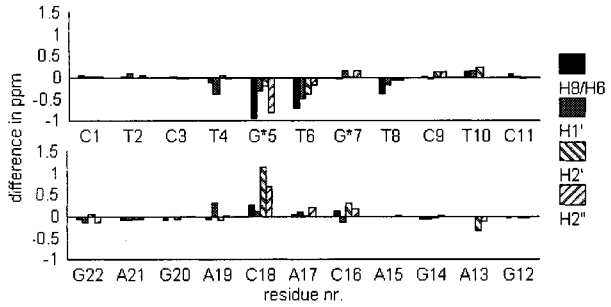

FIGURE 5: Graphical representation of the differences in chemical shift between the platinated duplex II and the unplatinated duplex I. The differences are shown for the aromatic, H1′, H2′, and H2″ protons. The largest differences are observed for residues G_5*, T_6, and C_{18}. This indicates a severe distortion of the 5′ side, and of the central thymine in the platinum lesion.

Three-Dimensional Structure of the Platinum 1,3-d(GTG) Intrastrand Cross-Link. The refined structure (Figure 6) reflected the features that were deduced from the qualitative inspection of the NOESY spectra discussed above. A family of 20 structures of the platinated duplex containing a 1,3-intrastrand cisplatin adduct was refined as described under Materials and Methods using a total of 1669 NOE restraints. Three of these structures were discarded on the basis of their high NMR *R* factors (large NOE violations resulting in simulated spectra different from the collected spectrum) and higher chemical energies. The resulting 17 structures all had an NMR *R* factor of 22% (the initial *R* factor was 78% for the starting structure). The agreement of the simulated and experimental spectra is illustrated in Figures 2, 4, and S5 (see Supporting Information). Due to the flexibility of the extruding T_6, and partly due to the small deviations in the exact helix curvature (vide infra), the 17 structures had an rmsd value for all heavy atoms of 1.3 Å (Figure S2). However, when the rmsd is calculated separately for the 5′-terminal and the 3′-terminal base pairs, the rmsd values are 0.5 and 0.6 Å, respectively, showing a good local convergence (see Figure S3). For the family of starting structures, the rmsd was 0.8 Å for the 5′ and the 3′ terminus. Global sugar conformations were identical in all refined structures, showing a clear alteration from the S type to the N type for the 5′G_5* and an intermediate conformation for T_6.

Although the duplex is still mainly in B-DNA conformation, the central G*TG* appears to be significantly distorted. A striking feature is that T_6, which is located between the two platinated guanines, is no longer stacked in any of the refined structures. This thymine is extruded into the minor groove of the helix. Figure 7 illustrates the flexibility of T6. Its position is not precisely determined by the NMR data, and this must be attributed to the flexibility of T_6 in solution, resulting in only weak NOE restraints for this thymine base. Only very weak NOEs are present in the methyl group of T_6. Not only is the sequential G_5*H6−T_6CH3 contact missing, but also the intraresidual contacts between T_6CH3 and the H1′, H2′/2″, and H3′ sugar protons are much smaller than the intraresidual contacts in the other thymines, which confirms that the T6 is actually extruded from the helix. The small sequential contacts of T_6CH3 with G_5* H1′, H2′/2″, H3′, and H4′ indicate that the thymine is directed toward the 5′-guanine. Since it is not restrained by stacking interactions or hydrogen bonding, T_6 is expected to show greater mobility compared to the other bases. This mobility is supported by the smaller line width of the methyl protons (14.6 Hz for T_6, and 16.5 and 22.0 Hz for T_4CH_3 and T_8-CH_3, respectively).

The refined structure shows that hydrogen bonding is lost for the G_5*-C_{18} and T_6-A_5 base pairs, and confirms the exchangeable proton data (vide supra). The 1,3-platinum cross-link induces a significant roll (60−80°) for the 5′G* and a smaller roll for the 3′G* (−12 to −20°) (Figure 6). It induces a bending of the helix toward the major groove of 27−33° in the calculated structures. The extruding T_6 and the local unwinding of the helix cause the minor groove to be shallow and widened in the G*TG* lesion. The width of the minor groove is in the range of 8.2−9.6 Å in the family of structures, but the average maximal minor groove width is about 8.5 Å. These values are intermediate compared to known values for B-DNA and A-DNA (Figure S4). Together with the differences in the position of the extruded central thymine, these minor groove widths illustrate the possible mobility in solution of the duplex.

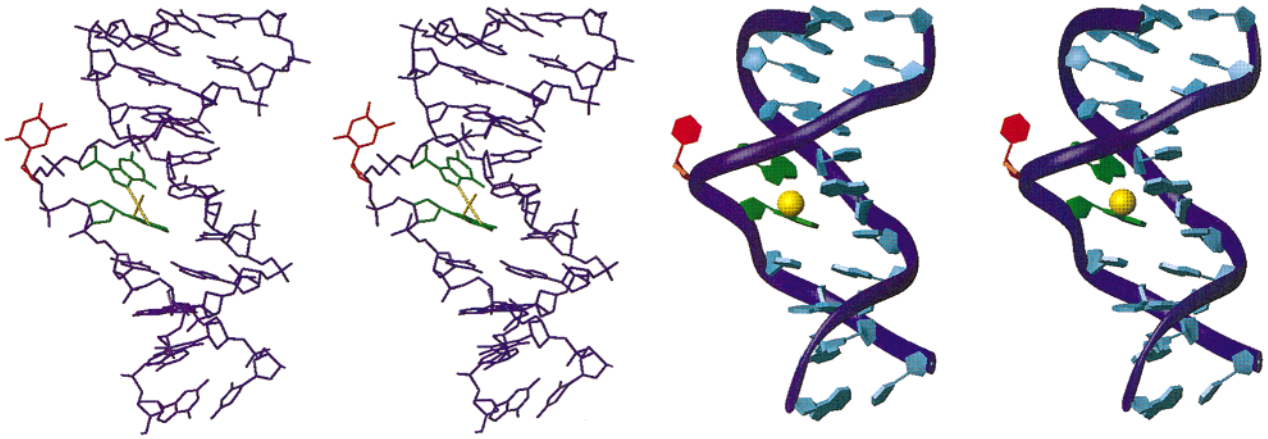

FIGURE 6: Stereoviews into the major groove of one final structure, created with the program Molmol (*37*). The structure is represented as a neon style figure (left) and schematically (right). The plots illustrate the structural distortions from B-DNA: (i) the bend toward the major groove; (ii) the unwinding of the helix at the site of the lesion; (iii) extrusion of the central thymine (shown in red) in the G*TG* lesion; (iv) inversion of the sugar geometry of the 5′-platinated guanine; (*v*) platinum atom coordination, causing the roll of the two coordinated guanines (shown in green).

FIGURE 7: Stereoview into the minor groove of the platinum lesion. This figure shows the three bases in the platinum lesion only. For clarity, 9 of 17 structures are shown superimposed on the planes of the guanine bases. This figure illustrates how the platinum atom induces a roll of the coordinated G_5* and G_7*, and the flexibility of T_6 (shown in red).

DISCUSSION

A family of 17 structures of the *cis*-diammineplatinum-(II) 1,3-d(GTG) intrastrand cross-link was calculated using the SPEDREF protocol. The calculated structures faithfully reflect the NOE data, which are represented by an *R* factor of 22%. The similarity of the collected and simulated spectra is illustrated in Figures 2, 4, and S5. Peaks g and h in Figure 2 are peaks that do not appear in the simulated spectrum. These arise from a small excess of ssIII and can be attributed to the H5/H6 cross-peaks of the ssIII cytosines. The structure is well determined except for the central thymine in the platinum lesion. The mobility of the T_6 in the family of calculated structures arises from the lack of NOE data restraining it to a fixed position in space. However, it is obvious that this thymine is extruded from the helix, since there are only few weak sequential NOE connectivities. The central thymine is mobile in solution, which also explains the absence of hydrogen bonds or stacking interactions.

The exact angle of curvature remains a problem for all DNA structures determined with NMR. Because of the absence of long-range constraints, there are no data which directly determine this angle. The angle reported for solution structures is dependent only on NOEs between neighboring bases, or in some cases on NOEs between bases separated by one base. One elegant way of overcoming this problem is employing paramagnetic restraints, as shown by Dunham et al. (*11*). They recently reported the structure of a spin-labeled cisplatinum derivative 1,2-d(GG) intrastrand adduct, which was refined using both paramagnetic and diamagnetic restraints (*11*).

In the family of structures of the platinum 1,3-(GTG) intrastrand adduct presented here, the bending of DNA is ~30°. The small variations in curvature as well as the flexibility of T_6 account for the rmsd value of 1.3 Å.

The structure presented here differs in three significant ways from the structure proposed by van Garderen and van Houten for the platinum 1,3-intrastrand cross-link in the similar duplex d(CTCTAGTGCTCAC)·d(GTGAGCACTAGAG) (*14*). This structure of the 1,3-intrastrand adduct employed different refinement techniques and a slightly different oligonucleotide. In that structure, the central thymine retained its stacking interactions with the 3′-platinated guanine, and this thymine was reported not to be extruded from the helix. The authors furthermore concluded (*14*) that the 5′ G-C base pair in the 1,3-cross-link was not dissociated; the third difference is the angle of curvature which was earlier reported to be ~20°. These differences can only partly be explained by the difference in sequence of the oligonucleotide. Van Garderen and van Houten used a 13-residue oligo which not only is 2 bases longer than the oligonucleotide used in our study, but also has 1 neighboring GC pair on the 3′ side of the lesion. The greater H-bonding capacity of this GC pair might allow less distortion. A second reason for the discrepancy might be the limited number of NOEs used. The authors report only 27 interresidual NOEs. Carefully examining these NOEs, we can conclude that actual data upon which both structures are based are actually more similar, although the final structures presented by van Garderen and van Houten and the ones presented in this paper differ significantly. Van Garderen and van Houten also observe no NOE from the central T methyl group to the H8 5′ neighboring G. Even more strikingly, they report the absence of any sequential cross-peak between the central T and the 3′G. Yet their model still presents the T as stacking, yielding distances in the model that would certainly give rise the above-mentioned missing cross-peaks. A factor adding to the discrepancy between the structures is related to the refinement procedure used. Earlier NMR studies used refinement protocols where NOE restraints were released during the last phases of the refinement.

The structure presented here agrees with earlier publications dealing with the structure of the 1,3-intrastrand adduct. An early NMR study by den Hartog et al. (*33*) revealed that the duplex is more distorted than the 1,2-d(GG) adduct, with the 5′G adopting an N-type conformation, and the central thymine was reported to be bulged out. Gel electrophoresis experiments indicated that the DNA duplex is bent by 23−35° (*34*−*36*). Additional chemical probing experiments confirmed that the 5′ side of the lesion is more distorted than the 3′ side, that base paring is disrupted for the 5′G*-C and the central T-A base pairs, and that the central thymine is exposed to the solvent (*34*). The structure presented here is in agreement with these studies: the thymine is extruded, the 5′G*-C and T-A base pairs are dissociated, and the angle of curvature is as expected.

Although the tertiary structures of platinum−DNA cross-links all contain similar features, the structural distortions induced by the *cis*-diammineplatinum(II) 1,3-d(GTG) intrastrand cross-link differ significantly from those induced by the 1,2-intrastrand d(GG) adduct. The inversion of the sugar pucker to an N-type configuration of the 5′-platinated guanine ribose is a uniform feature of platinum−DNA intrastrand adducts (*7*, *8*, *11*). N-type sugar is commonly seen for A-DNA. The inversion of the sugar conformation is accompanied by a broadening of the minor groove to a value intermediate of the values for B-DNA and A-DNA. The global conformational change for the 1,3-d(GG) adduct is also characterized by the extruding thymine. The 1,3-intrastrand lesion causes the duplex to bend toward the major groove by ~30°; although the distortion induced by the 1,3-intrastrand cross-link is quite severe compared to the 1,2-intrastrand cross-link, the bending induced by the platinum lesion is less profound compared to the 55−78° kink induced by the 1,2-d(GG) intrastrand link. This degree of bending might be very important for the biological implication of a platinum−DNA adduct. Gelasco and Lippard (*8*) reported a great similarity between the structure of the 1,2-d(GG) intrastrand adduct and the structures of the DNA complexes of the HMG proteins SRY and LEF-1, which induce a similar bending angle in the DNA as the platinum intrastrand adduct.

The much less severe binding of the platinum 1,3-intrastrand adduct might explain why this class of proteins selectively recognizes the 1,2-intrastrand adducts (*17*, *18*).

Concluding Remarks. In conclusion, the structure of the platinum 1,3-d(GTG) intrastrand adduct has been determined, and it is severely distorted from B-DNA. Although it shares common features with the reported structures of the platinum 1,2-d(GG) intrastrand cross-link, such as the widening of the minor groove at the site of the lesion and reversal of the 5′ sugar pucker, it is clear that these distortions are different compared to the 1,2-d(GG) adduct. The distortion is spread out over the entire lesion, and is most severe on the 5′ side. The 5′G-C and the central T-A base pairs are disrupted. The central thymine in the G*TG* lesion is bulged out of the helix which is unwound and kinked by ∼30°. Unlike the structures of the 1,2-d(GG) adduct, the structure reported here for the 1,3-intrastrand adduct does not resemble the known structures of DNA complexes of the HMG proteins (*7*). This difference may explain why these proteins, that efficiently recognize the 1,2-intrastrand adducts, do *not* recognize the 1,3-intrastrand adduct.

ACKNOWLEDGMENT

This work has been performed under the auspices of the BIOMAC Research Graduate School of Leiden University and Delft Technical University. We thank Johnson & Matthey for their generous loan of K_2PtCl_4.

SUPPORTING INFORMATION AVAILABLE

Stacked plots of the H8/H6 to H3′ region of the simulated and recorded NOESY spectra, a Molmol representation of the family of structures, a plot of the average minor groove width, and contour plots of the entire recorded and simulated NOESY spectra (7 pages). This material is available free of charge via the Internet at http://pubs.acs.org.

REFERENCES

1. Reedijk, J. (1996) *Chem. Commun.*, 801−806.
2. Chu, G. (1994) *J. Biol. Chem. 269*, 787−790.
3. Fichtinger-Schepman, A. M. J., van der Veer, J. L., den Hartog, J. H. J., Lohman, P. H. M., and Reedijk, J. (1985) *Biochemistry 24*, 707−713.
4. Blommaert, F. A., van Dijk-Knijnenburg, H. C. M., Dijt, F. J., den Engelse, L., Baan, R. A., Berends, F., and Fichtinger-Schepman, A. M. J. (1995) *Biochemistry 34*, 8474−8480.
5. Fichtinger-Schepman, A. M. J., van Dijk-Knijnenburg, H. C. M., van der Velde-Visser, S. D., Berends, F., and Baan, R. (1995) *Carcinogenesis 16*, 2447−2453.
6. Yang, D., and Wang, A. H.-J. (1996) *Prog. Biophys. Mol. Biol. 66*, 81−111.
7. Yang, D., van Boom, S. S. G. E., Reedijk, J., van Boom, J. H., and Wang, A. H.-J. (1995) *Biochemistry 34*, 12912−12921.
8. Gelasco, A., and Lippard, S. J. (1998) *Biochemistry 37*, 9230−9239.
9. Takahara, P. M., Rosenzweig, A. C., Frederick, C. A., and Lippard, S. J. (1995) *Nature 377*, 649−652.
10. Takahara, P. M., Frederick, C. A., and Lippard, S. J. (1996) *J. Am. Chem. Soc. 118*, 12309−12321.
11. Dunham, S. U., Dunham, S. U., Turner, C. J., and Lippard, S. J. (1995) *J. Am. Chem. Soc. 120*, 5395−5406.
12. Huang, H., Zhu, L., Reid, B. R., Drobny, G. P., and Hopkins, P. B. (1995) *Science 270*, 1842−1845.
13. Paquet, R. F., Perez, C., Leng, M., Lancelot, G., and Malinge, J.-M. (1996) *J. Biomol. Struct. Dyn. 14*, 67−77.
14. van Garderen, C. J., and van Houte, L. P. A. (1994) *Eur. J. Biochem. 225*, 1169−1179.
15. Bauer, C., Peleg-Schulman, T., Gibson, D., and Wang, A. H.-J. (1998) *Eur. J. Biochem. 256*, 253−260.
16. Yang, D., van Boom, S. S. G. E., Reedijk, J., van Boom, J. H., Farell, N., and Wang, A. H.-J. (1995) *Nat. Struct. Biol. 2*, 577−585.
17. Pil, P. M., and Lippard, S. J. (1992) *Science 256*, 234−237.
18. Chow, C. S., Barnes, C. M., and Lippard, S. J. (1995) *Biochemistry 34*, 2956−2964.
19. Trimmer, E. E., Zamble, D. B., Lippard, S. J., and Essigman, J. M. (1998) *Biochemistry 37*, 352−362.
20. Donahue, B. A., Augot, M., Bellon, S. F., Treiber, D. K., Toney, J. H., Lippard, S. J., and Essigman, J. M. (1990) *Biochemistry 29*, 5872−5880.
21. Visse, R., van Gool, A. J., Moolenaar, G. F., de Ruijter, M., and van de Putte, P. (1994) *Biochemistry 33*, 1804−1811.
22. Robinson, H., and Wang, A. H.-J. (1992) *Biochemistry 31*, 3524−3533.
23. Dhara, S. C. (1970) *Ind. J. Chem. 8*, 193.
24. Sklenar, V., Piotto, M., Leppik, R., and Saudek, V. (1993) *J. Magn. Reson. 102*, 241−245.
25. Kraulis, P. J. (1989) *J. Magn. Reson. 24*, 627−633.
26. Brünger, A. T. (1992) *X-plor version 3.1. A System for X-ray Crystallography and NMR*, Yale University Press, New Haven, CT.
27. Herman, F., Kozelka, J., Stoven, V., Guittet, E., Girault, J.-P., Huynh-Dinh, T., Igolen, J., Lallemand, J. Y., and Chottard, J.-C. (1990) *Eur. J. Biochem. 194*, 119−133.
28. Post, C. B., Meadows, R. P., and Gorestein, D. G. (1990) *J. Am. Chem. Soc. 112*, 6796−6803.
29. Akkerman, M. A., Haasnoot, C. A., and Hilbers, C. W. (1988) *Eur. J. Biochem. 173*, 211−225.
30. Akkerman, M. A., Neijman, E. W., Wijmenga, S. S., Hilbers, C. W., and Bermel, C. W. (1990) *J. Am. Chem. Soc. 117*, 7462−7474.
31. Hare, D. R., Wemmer, D. E., Chow, S.-H., Droby, G., and Reid, B. (1983) *J. Mol. Biol. 171*, 319−336.
32. Wijmenga, S. S., Mooren, M. M. W., and Hilbers, C. W. (1993) in *NMR of Macromolecules: A practial Approach* (Roberts, G. C. K., Ed.) Oxford University Press Inc., New York.
33. den Hartog, J. H. J., Altona, C., van den Elst, H., van der Marel, G., and Reedijk, J. (1985) *Inorg. Chem. 24*, 983−986.
34. Marrot, L., and Leng, M. (1989) *Biochemistry 28*, 1454−1461.
35. Anin, M.-F., and Leng, M. (1990) *Nucleic Acids Res. 18*, 4395−4400.
36. Bellon, S. F., and Lippard, S. J. (1990) *Biophys. Chem. 35*, 179−188.
37. Koradi, R., Billeter, M., and Wüthrich, K. (1996) *J. Mol. Graphics 14*, 51−55.
38. Coste, J., Malinge, J.-M., Serre, L., Shepard, W., Roth, M., Leng, M., and Zelwer, C. (1999) *Nucleic Acids Res. 27*, 1837−1846.
39. Ohndorf, U.-M., Rould, M. A., He, Q., Pabo, C. O., and Lippard, S. J. (1999) *Nature 339*, 708−712.

BI9904757